Title

Templated Growth of a Spin-Frustrated Cluster Fragment of MnBr2 in a Metal—Organic Framework

Journal

Inorganic Chemistry, 60(21)

ISSN

0020-1669

Authors

Turkiewicz, Ari
Tomlinson, Warren
Gonzalez, Miguel I
et al.

Publication Date

2021-11-01

DOI

10.1021/acs.inorgchem.1c01345

Templated growth of a spin-frustrated cluster fragment of $MnBr_2$ in a metal–organic framework

Ari B. Turkiewicz,[†] Warren Tomlinson,[‡] Miguel I. Gonzalez,[†∥] Joseph Hooper,[‡] and Jeffrey R. Long*[†§⊥]

[†]Department of Chemistry, and [§]Department of Chemical & Biomolecular Engineering, University of California, Berkeley, California 94720, United States

[‡]Department of Physics, Naval Postgraduate School, Monterey, California 93943, United States

[⊥]Materials Sciences Division, Lawrence Berkeley National Laboratory, Berkeley, California 94720, United States

The metal–organic framework $Zr_6O_4(OH)_4(bpydc)_6$ ($bpydc^{2-}$ = 2,2′-bipyridine-5,5′-dicarboxylate) is used to template the growth of a cluster fragment of the two-dimensional solid $MnBr_2$, which was predicted to exhibit spin frustration. Single-crystal and powder X-ray diffraction analyses reveal a cluster with 19 metal ions arranged in a triangular lattice motif. Static magnetic susceptibility measurements indicate antiferromagnetic coupling between the high-spin (S = $^5/_2$) Mn^{II} centers, and dynamic magnetic susceptibility data suggest population of low-lying excited states, consistent with magnetic frustration. Density functional theory calculations are used to determine the energies for a subset of the thousands of magnetic configurations available to the cluster. The Yamaguchi generalized spin-projection method is then employed to construct a model for the magnetic coupling interactions within the cluster, enabling facile determination of the energy for all possible magnetic configurations. The confined cluster is predicted to possess a doubly degenerate, highly geometrically frustrated ground state with a total spin of S_{Total} = $^5/_2$.

Magnetic molecules exhibiting spin frustration have gained increasing attention for hosting unique physical properties.[1] For instance, the chiral spin states of frustrated triangular clusters have been proposed as an alternative means for encoding spin qubits.[2,3] Additionally, these molecules can serve as models for bulk materials, supplementing our understanding of non-trivial magnetic order in spin frustrated systems such as spin liquids.[4,5]

Geometric spin frustration arises in both molecules and bulk materials due to competing antiferromagnetic interactions that cannot be simultaneously satisfied. For example, two-dimensional triangular[6] and Kagomé[7,8] lattices and three-dimensional hyperkagome[9] and pyrochlore[10] lattices can all provide platforms for studying spin frustration in bulk materials. In addition, molecular systems featuring odd-numbered metal rings,[11] cuboctahedra and icosidodecahedra,[12,13] and disc-like clusters with triangular motifs[14–18] have all demonstrated spin frustration effects. The magnitude of the spin on the individual magnetic centers themselves is also important in these frustrated systems. For spin liquids, most research has focused on magnetic centers with spin, S, or total angular momentum, J, values of $^1/_2$, which are least likely to afford long-range ordered, commensurate ground states.[6-10] However, higher-spin systems can also afford interesting phenomena such as spin chirality.[19]

Recently, we reported a series of metal halide clusters of the type $M_{19}X_{38}$ (M = Fe, Co, Ni; X = Cl, Br) confined within the metal–organic framework $Zr_6O_4(OH)_4(bpydc)_6$ (**1**).[20] Notably, single-crystal X-ray diffraction characterization of all the clusters revealed a triangular lattice akin to a single layer of the corresponding bulk metal dihalide. The intralayer ferromagnetic coupling characteristic of the bulk metal halides is also retained in these clusters and gives rise to high-spin ground states. Given the close relationship between the atomic and magnetic structures of these clusters and those of their parent materials, we sought to assemble analogous framework-confined clusters with antiferromagnetically coupled metal ions to prepare a magnetically frustrated system. We identified $MnBr_2$ as a promising target, given that it is a bulk antiferromagnet constructed from S_{Mn} = $^5/_2$ spin centers on a triangular lattice and it crystallizes in the layered CdI_2 structure type.[21] Of note, although they have not yet been isolated, monolayers of $MnBr_2$ are predicted to be exfoliable, antiferromagnetic semiconductors.[22] This templating approach therefore offers a powerful opportunity to study magnetic frustration and underlying coupling interactions in a technologically relevant material. Several manganese-based, disc-like clusters have been

reported, most of which are hydroxo-bridged, mixed-valent clusters, although these have generally been designed to maximize spin rather than to engender frustration effects.[23] At least two homo-valent $\{Mn^{II}_7\}$ disc-like clusters have been reported and interestingly both exhibit spin frustration.[17,18] Additionally, the one-dimensional solid $\{Mn_4Cl_8(THF)_6(Mn(THF)_2Cl_2\}_\infty$ contains tetranuclear Mn^{II} clusters, and all spin centers in the material engage in antiferromagnetic coupling.[24]

Treatment of single crystals of **1** with 19 equiv. of $MnBr_2$ in a 1:10 v/v mixture of acetonitrile and toluene affords **1**$(MnBr_2)_{11}$. Single-crystal X-ray diffraction characterization revealed a structure containing 19 total manganese positions arranged in a triangular lattice to afford 24 triangular circuits (Figure 1). While the triangular circuits are not themselves equilateral, the crystal structure space group

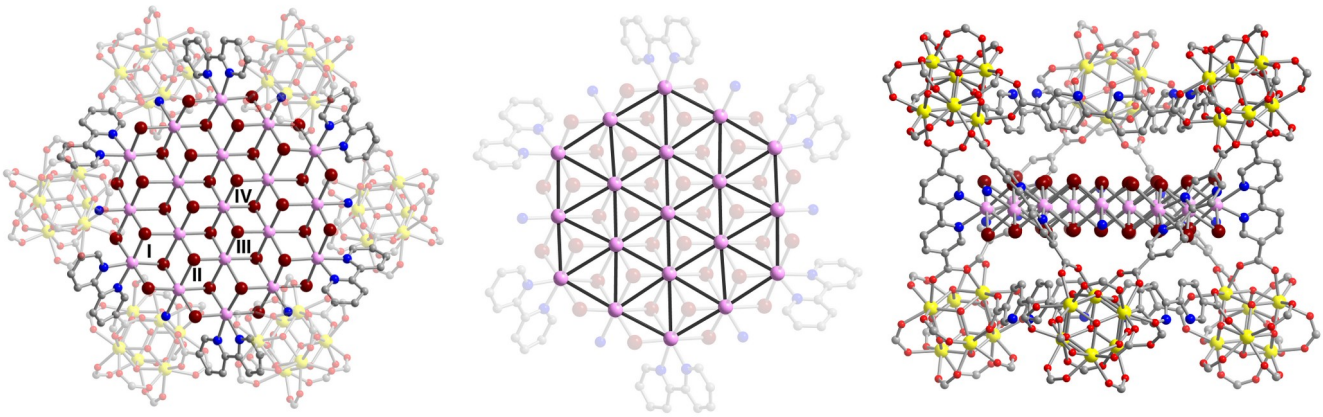

Figure 1. Portions of the crystal structure of **1**$(MnBr_2)_{11}$ at 100 K as determined from single-crystal X-ray diffraction. (Left) Top-down view of the templated cluster, which features 19 Mn^{II} ions arranged in a triangular lattice. The four crystallographically distinct Mn^{II} sites are labelled with roman numerals. (Middle) Cluster view highlighting the triangular lattice of Mn atoms. (Right) Cluster side view. Yellow, pink, dark red, red, blue and grey spheres represent Zr, Mn, Br, O, N and C atoms, respectively; H atoms and outer sphere Br anions are omitted for clarity.

symmetry of $Pa\bar{3}$ enforces a local D_{3d} point group symmetry for the cluster. Four of the 19 manganese positions are crystallographically distinct. Sites I and II each generate six symmetrically equivalent positions that together comprise the outer ring of the cluster. Site I is bound to the bipyridine moiety of the framework, and site II bridges adjacent site I positions. Site III consists of six equivalent positions that comprise the inner ring of the cluster, and site IV is the central Mn^{II} ion. The site occupancies are highest at the cluster edges and decrease toward the center, with values of 0.864(12), 0.625(12), 0.382(12), and 0.25(3) for sites I–IV, respectively. Close examination of the crystal structure reveals that site II adopts a pseudo-octahedral $MnBr_5(MeCN)$ coordination environment, but it was only possible to resolve the nitrogen atom of the acetonitrile ligand. At full occupancy, the cluster can therefore be described as the divalent cation $Mn_{19}Br_{36}(bpydc)_6(MeCN)_6^{2+}$ with two additional outer-sphere bromide anions (Figure S1).

Treatment of microcrystalline **1** with 19 equiv. of $MnBr_2$ under identical synthetic conditions as used for the single crystals afforded **1**$(MnBr_2)_{14}$ with a higher overall metal occupancy (73.3(2)%), as determined using inductively coupled plasma-optical emission spectroscopy. Further characterization of **1**$(MnBr_2)_{14}$ by powder X-ray diffraction (Figure S2) as well as scanning electron microscopy and energy-dispersive X-ray spectroscopy (Figures S3 and 4) confirmed sample purity and uniform incorporation of $MnBr_2$. The smaller particle sizes of microcrystalline **1** may facilitate the increased metal loading relative to that determined for the single crystals. The use of more than 19 equiv. of $MnBr_2$ did not increase the metal loading achievable in single-crystalline or microcrystalline **1**.

At full occupancy, the $Mn_{19}Br_{36}$ cluster corresponds to a fragment excised from a single layer of the bulk $MnBr_2$ solid-state structure. The average nearest neighbor Mn···Mn distance in the cluster is 3.74(6) Å, which is slightly compressed relative to that in the bulk material (3.922 Å).[21] The rigidity of the framework likely enforces the compressed cluster geometry, despite the ability of the framework linkers to accommodate minor strain. The Mn–Br–Mn bond angles of the cluster range from 87.2(2) to 92.8(2)°, compared with 90° in the bulk material. Bulk $MnBr_2$ adopts an antiferromagnetically ordered state below 2.16 K, wherein each $MnBr_2$ layer consists of two-metal atom wide ferromagnetic stripes with antiferromagnetic coupling between neighboring stripes. Further antiferromagnetic order exists between layers.[21,25,26] However, this spin texture does not necessarily translate to a discrete cluster. In the bulk material, there are several competing exchange mechanisms between nearest neighbors, including antiferromagnetic

direct exchange as well as ferromagnetic and antiferromagnetic superexchange.[27,28] Manganese dihalides have also been shown to exhibit significant coupling between second-nearest and even third-nearest neighbors.[29] Consequently, the ground state magnetic structure for a finite-sized $MnBr_2$ cluster will be highly sensitive to Mn···Mn distances and Mn–Br–Mn bond angles.

Dc magnetic susceptibility data were collected to probe the magnetic interactions present in microcrystalline **1**$(MnBr_2)_{14}$ (Figure 2a). At 300 K, the product of molar magnetic susceptibility and temperature ($\chi_M T$) is 59.4 emu K mol^{-1}, which corresponds well to the expected value for 14 uncoupled, high-spin Mn^{II} ions (61.25 emu K mol^{-1} assuming $g = 2.00$). The magnitude of $\chi_M T$ decreases as the temperature is lowered, indicative of antiferromagnetic coupling between manganese centers. This conclusion is further supported by the negative Weiss temperature of −27.2 K determined from a Curie-Weiss fit to $1/\chi_M$ collected under a 0.01 T field (Figure S5). Variable-field magnetization data collected at 2 K feature minimal curvature, and at the highest field of 7 T, M reaches a value of only 30.9 μ_B (Figure 2b). This value is approximately half that expected for parallel alignment of all Mn spins (70 μ_B), again supporting the presence of antiferromagnetic coupling between Mn^{II} centers. In tandem with the triangular cluster lattice, these dominant antiferromagnetic interactions are expected to give rise to geometric frustration in **1**$(MnBr_2)_{14}$. However, multiple weak coupling interactions between Mn^{II} centers are likely to give rise to many low-lying excited states that complicate experimental validation of the total ground state spin (S_{Total}).[23,30] In some situations, collecting reduced magnetization data at low applied fields and temperatures has been shown to mitigate this difficulty.[14,31] In this case, however, we were unable to obtain satisfactory fits to reduced magnetization data collected for microcrystalline **1**$(MnBr_2)_{14}$ under fields ranging from 0.1 to 2.0 T and temperatures from 2.0 to 10 K (Figure S6).

Ac magnetic susceptibility data collected under zero applied field can offer insight into ground state spin population and magnitude, as the absence of an applied field mitigates the approach or crossing of excited states with the ground state.[31] In particular, the product of the in-phase molar magnetic susceptibility with temperature ($\chi_M'T$) will be temperature-independent if the ground state is exclusively populated, whereas this product will be temperature-dependent if there is also excited

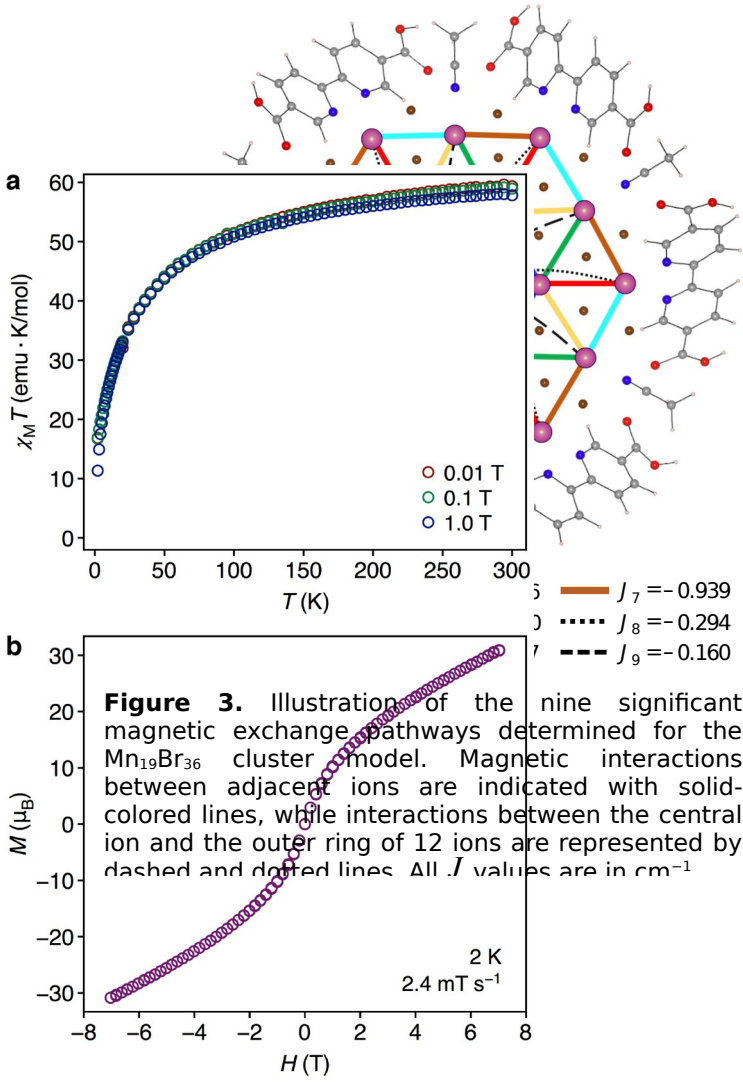

Figure 3. Illustration of the nine significant magnetic exchange pathways determined for the $Mn_{19}Br_{36}$ cluster model. Magnetic interactions between adjacent ions are indicated with solid-colored lines, while interactions between the central ion and the outer ring of 12 ions are represented by dashed and dotted lines. All J values are in cm^{-1}.

state population. Ac susceptibility data were collected for **1**$(MnBr_2)_{14}$ between 2 and 10 K using a 4 Oe field oscillating at frequencies from 1–500 Hz (Figures S7 and 8). No out-of-phase signal (χ_M'') was detected, but the corresponding plot of $\chi_M'T$ versus T is clearly temperature-dependent (Figure S9), consistent with population of low-lying excited states. Similar behavior attributable to low-lying excited states was reported for disc-like Mn^{II}_7 clusters.[17,18]

To probe the magnetic interactions and ground state structure of **1**$(MnBr_2)_{14}$ further, we turned to computational methods. A $Mn_{19}Br_{36}$ cluster model was constructed using atomic coordinates from

the single-crystal structure of **1**$(MnBr_2)_{11}$, including bipyridine and acetonitrile ligands but excluding the zirconium framework nodes and the two outer sphere bromide anions. The structure was treated as a +2 cation with the central Mn^{2+} ion holding the excess charge to maintain symmetry. Together, these elements preserve the essential features of **1**$(MnBr_2)_{11}$. We then constructed 18 representative magnetic configurations (Figures S10-S27) and determined the energy (E) and total spin magnitude ($\langle S^2_{Total} \rangle$) for each configuration using density functional theory (DFT) calculations performed with the Minnesota M11L meta-GGA functional.[32] By examining the spin flips and associated energy differences between pairs of magnetic configurations, we deduced nine significant coupling interactions, namely between adjacent metal ions and between the central metal ion and outer ring of 12 metal ions (see the Supporting Information for details).

We then employed the Yamaguchi generalized spin-projection (GP) method for multi-spin systems[33] to first isolate all nine antiferromagnetic spin correlation functions $^{AF}\langle S_i \cdot S_j \rangle$ via the solution to a series of ten linear equations for $\langle S^2_{Total} \rangle$ (Table S4). The correlation functions determined in this way were all found to differ by less than 0.1% from the value of $-|S_i| \cdot |S_j|$ (here, –6.25 for S_{Mn} = $^5/_2$), which indicates virtually no orbital overlap between Mn^{II} centers and is unsurprising, given the average distance of ~3.74 Å between adjacent metal sites. Using $-|S_i| \cdot |S_j|$ for our spin correlation functions, we then constructed a series of 18 linear equations of the form[33]

$$E = E_0 - 2\sum_{\alpha} J_{\alpha} \sum_{\langle i,j \rangle} \langle S_i \cdot S_j \rangle \quad (1)$$

where E is the energy for a particular magnetic configuration determined by DFT, J_α sums over the nine coupling constants, and $S_i \cdot S_j$ sums over the six pairs of Mn^{II} centers associated with each J. Using these equations, we fit nine different J values and a value for E_0. A comparison of the original DFT energies with those output by the multiple linear regression analysis (see Table S5 and Figure S28) indicates the strength of this nine-J model for the magnetic interactions of the cluster. All interactions are found to be antiferromagnetic with the strongest interactions toward the center of the cluster (Figure 3). With these J-constants in hand, it was then possible to use eq 1 to reliably predict the energy of any other magnetic configuration, without additional DFT calculations.

With 19 manganese centers in the core of the cluster, there are hundreds of thousands of possible spin configurations. We fixed the central ion as "spin up" and iterated through all 2^{18} different spin configurations, calculated the energy of each via eq 1. The resulting pairs of spin and energy were further reduced by eliminating all repeated instances of combined spin and energy to afford 9,500 distinct combinations (Figure S29). The resulting energy level diagram, a portion of which is shown in Figure 4a, reveals numerous low-lying excited state configurations that are consistent with the temperature dependence of the ac magnetic susceptibility data. Finally, we identified a doubly-degenerate, highly-geometrically frustrated ground state configuration with a total spin of S_{Total} = $^5/_2$ (Figure 4b). Overall, there are 18 pairs of frustrated interactions in the ground state: three between the central ion and the ions of the middle ring, six between the central ion and ions of the outer ring, and nine between the middle and outer rings of ions.

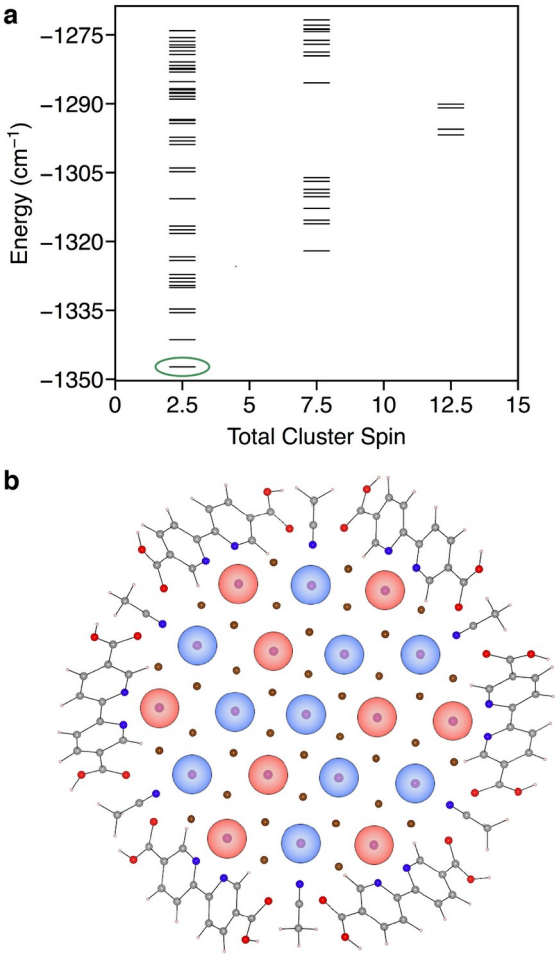

Figure 2. (a) Plot of $\chi_M T$ versus T data for **1**$(MnBr_2)_{14}$ under applied fields of 0.01, 0.1 and 1.0 T. (b) Magnetization versus applied field data for

The foregoing results illustrate the utility of using metal–organic frameworks as ligand templates to target clusters with specific structures and properties. Using **1**, we were able to template and confine the growth of a rare two-dimensional, homovalent Mn^{II} cluster that also exhibits spin frustration. Calculations performed for a representative $Mn_{19}Br_{36}^{2+}$ cluster fragment predict a ground state magnetic configuration that is notably distinct from the striped antiferromagnetic phase of bulk $MnBr_2$. This result

further suggests that isolating monolayers of $MnBr_2$ may be an interesting research direction and that its magnetic properties could be affected by modulating lattice and exchange parameters.

ASSOCIATED CONTENT

Supporting Information

The Supporting Information is available free of charge on the ACS Publications website.

Additional experimental and computational details, powder X-ray diffraction data; single-crystal X-ray diffraction data; magnetic susceptibility data; electron microscopy data; and additional references. (PDF)

Crystallographic data **1**$(MnBr_2)_{11}$ (CIF)

AUTHOR INFORMATION

Corresponding Author

* jrlong@berkeley.edu

Present Addresses

[‖]Department of Chemistry and Chemical Biology, Harvard University, 12 Oxford Street, Cambridge, Massachusetts 02138, United States.

Notes

The authors declare no competing financial interest.

ACKNOWLEDGMENT

This research was supported through a Multidisciplinary University Research Initiatives Program funded by the U.S. Department of Defense, Office of Naval Research under Award N00014-15-1-2681. Single-crystal X-ray diffraction experiments were performed at beamline 11.3.1 at the Advanced Light Source at Lawrence Berkeley National Laboratory. The Advanced Light Source is supported by the Director, Office of Science, Office of Basic Energy Sciences, of the U.S. Department of Energy under Contract no. DE-AC02-05CH11231. We thank the U.S. National Science Foundation for providing graduate fellowship support for A.B.T. In addition, we thank Dr. Simon J. Teat for experimental assistance and helpful discussions and Dr. Katie R. Meihaus for editorial assistance.

Figure 4. (a) Subset of energy levels within 75 cm^{-1} of the ground state, as computed using eq 1. Energy levels were adjusted so the high-spin state of $S_{Total} = {}^{95}/_{2}$ is at 0 cm^{-1}. The ground state is indicated by a green ellipse. (b) Ground state magnetic configuration. Ions shaded in blue correspond to spin up, Ions shaded in red correspond to spin down.

REFERENCES

(1) Schnack, J. Effects of Frustration on Magnetic Molecules: A Survey from Oliver Kahn Until Today. *Dalt. Trans.* **2010**, *39*, 4677–4686.

(2) Ghirri, A.; Van Tol, J.; Vitorica-Yrezabal, I.; Timco, G. A.; Winpenny, R. E. P. Effects of the Dzyaloshinskii-Moriya Interaction in Cr_3 Triangular Spin Clusters Detected by Specific Heat and Multi-Frequency Electron Spin Resonance. *Dalt. Trans.* **2015**, *44* (31), 14027–14033.

(3) Troiani, F.; Stepanenko, D.; Loss, D. Hyperfine-Induced Decoherence in Triangular Spin-Cluster Qubits. *Phys. Rev. B - Condens. Matter Mater. Phys.* **2012**, *86* (16), 1–5.

(4) Waldmann, O.; Stamatatos, T. C.; Christou, G.; Güdel, H. U.; Sheikin, I.; Mutka, H. Quantum Phase Interference and Néel-Vector Tunneling in Antiferromagnetic Molecular Wheels. *Phys. Rev. Lett.* **2009**, *102* (15), 18–22.

(5) Baker, M. L.; Guidi, T.; Carretta, S.; Ollivier, J.; Mutka, H.; Güdel, H. U.; Timco, G. A.; Mcinnes, E. J. L.; Amoretti, G.; Winpenny, R. E. P.; Santini, P. Spin Dynamics of Molecular Nanomagnets Unravelled at Atomic Scale by Four-Dimensional Inelastic Neutron Scattering. *Nat. Phys.* **2012**, *8* (12), 906–911.

(6) Yamashita, M.; Nakata, N.; Senshu, Y.; Nagata, M.; Yamamoto, H. M.; Kato, R.; Shibauchi, T.; Matsuda, Y. Highly Mobile Gapless Excitations in a Two-Dimensional Candidate Quantum Spin Liquid. *Science* **2010**, *328* (5983), 1246–1248.

(7) Shores, M. P.; Nytko, E. A.; Bartlett, B. M.; Nocera, D. G. A Structurally Perfect S = 1/2 Kagomé Antiferromagnet. *J. Am. Chem. Soc.* **2005**, *127* (39), 13462–13463.

(8) Banerjee, A.; Bridges, C. A.; Yan, J. Q.; Aczel, A. A.; Li, L.; Stone, M. B.; Granroth, G. E.; Lumsden, M. D.; Yiu, Y.; Knolle, J.; Bhattacharjee, S.; Kovrizhin, D. L.; Moessner, R.; Tennant, D. A.; Mandrus, D. G.; Nagler, S. E. Proximate Kitaev Quantum Spin Liquid Behaviour in a Honeycomb Magnet. *Nat. Mater.* **2016**, *15* (7), 733–740.

(9) Okamoto, Y.; Nohara, M.; Aruga-Katori, H.; Takagi, H. Spin-Liquid State in the S=1/2 Hyperkagome Antiferromagnet $Na_4Ir_3O_8$. *Phys. Rev. Lett.* **2007**, *99* (13), 4–7.

(10) Rau, J. G.; Gingras, M. J. P. Frustrated Quantum Rare-Earth Pyrochlores. *Annu. Rev. Condens. Matter Phys.* **2019**, *10* (1), 357–386.

(11) Woolfson, R. J.; Timco, G. A.; Chiesa, A.; Vitorica-Yrezabal, I. J.; Tuna, F.; Guidi, T.; Pavarini, E.; Santini, P.; Carretta, S.; Winpenny, R. E. P. $[CrF(O_2C^tBu)_2]_9$: Synthesis and Characterization of a Regular Homometallic Ring with an Odd Number of Metal Centers and Electrons. *Angew. Chemie - Int. Ed.* **2016**, *55* (31), 8856–8859.

(12) Blake, A. J.; Gould, R. O.; Grant, C. M.; Milne, P. E. Y.; Parsons, S.; Winpenny, R. E. P. Reactions of Copper Pyridonate Complexes with Hydrated Lanthanoid Nitrates. *J. Chem. Soc., Dalt. Trans* **1997**, 485–495.

(13) Müller, A.; Luban, M.; Schröder, C.; Modler, R.; Kögerler, P.; Axenovich, M.; Schnack, J.; Canfield, P.; Bud'ko, S.; Harrison, N. Classical and Quantum Magnetism in Giant Keplerate Magnetic Molecules. *ChemPhysChem* **2001**, *2* (8–9), 517–521.

(14) Stamatatos, T. C.; Foguet-Albiol, D.; Poole, K. M.; Wernsdorfer, W.; Abboud, K. A.; O'Brien, T. A.; Christou, G. Spin Maximization from S = 11 to S = 16 in Mn_7 Disk-like Clusters: Spin Frustration Effects and Their Computational Rationalization. *Inorg. Chem.* **2009**, *48* (20), 9831–9845.

(15) Deng, Y. K.; Su, H. F.; Xu, J. H.; Wang, W. G.; Kurmoo, M.; Lin, S. C.; Tan, Y. Z.; Jia, J.; Sun, D.; Zheng, L. S. Hierarchical Assembly of a $\{Mn^{II}_{19}Mn^{III}_4\}$ Brucite Disc: Step-by-Step Formation and Ferrimagnetism. *J. Am. Chem. Soc.* **2016**, *138* (4), 1328–1334.

(16) Mukherjee, S.; Bagai, R.; Abboud, K. A.; Christou, G. Raising the Spin of Fe^{III}_7 Disklike Clusters: The Power of Molecular Spin Frustration. *Inorg. Chem.* **2011**, *50* (9), 3849–3851.

(17) Vignesh, K. R.; Langley, S. K.; Murray, K. S.; Rajaraman, G. What Controls the Magnetic Exchange Interaction in Mixed- and Homo-Valent Mn_7 Disc-like Clusters? A Theoretical Perspective. *Chem. - A Eur. J.* **2015**, *21* (7), 2881–2892.

(18) Langley, S. K.; Chilton, N. F.; Massi, M.; Moubaraki, B.; Berry, K. J.; Murray, K. S. Synthesis and Characterization of Homo- and Heterovalent Tetra- Hexa- Hepta- and Decanuclear Manganese Clusters Using Pyridyl Functionalized β-Diketone, Carboxylate and Triethanolamine Ligands. *Dalt. Trans.* **2010**, *39* (31), 7236–7249.

(19) Grohol, D.; Matan, K.; Cho, J. H.; Lee, S. H.; Lynn, J. W.; Nocera, D. G.; Lee, Y. S. Spin Chirality on a Two-Dimensional Frustrated Lattice. *Nat. Mater.* **2005**, *4* (4), 323–328.

(20) Gonzalez, M. I.; Turkiewicz, A. B.; Darago, L. E.; Oktawiec, J.; Bustillo, K.; Grandjean, F.; Long, G. J.; Long, J. R. Confinement of Atomically Defined Metal Halide Sheets in a Metal–Organic Framework. *Nature* **2020**, *577* (7788).

(21) Wollan, E. O.; Koehler, W. C.; Wilkinson, M. K. Neutron Diffraction Study of the Magnetic Properties of $MnBr_2$. *Phys. Rev.* **1958**, *110* (3), 638–646.

(22) Mounet, N.; Gibertini, M.; Schwaller, P.; Campi, D.; Merkys, A.; Marrazzo, A.; Sohier, T.; Castelli, I. E.; Cepellotti, A.; Pizzi, G.; Marzari, N. Two-Dimensional Materials from High-Throughput Computational Exfoliation of Experimentally Known Compounds. *Nat. Nanotechnol.* **2018**, *13* (3), 246–252.

(23) Stamatatos, T. C.; Christou, G. Mixed Valency in Polynuclear Mn^{II}/Mn^{III}, Mn^{III}/Mn^{IV} and $Mn^{II}/Mn^{III}/Mn^{IV}$ Clusters: A Foundation for High-Spin Molecules and Single-Molecule Magnets. *Philos. Trans. R. Soc. A Math. Phys. Eng. Sci.* **2008**, *366* (1862), 113–125.

(24) Zhao, H.; Clérac, R.; Sun, J. S.; Ouyang, X.; Dunbar, K. R.; Clemente-Juan, J. M.; Gómez-García, C. J.; Coronado, E. A Comparative Structural and Magnetic Study of Three Compounds Based on the Cluster Unit $M_4Cl_8(THF)_6$ (M = Mn, Fe, Co). *J. Solid State Chem.* **2001**, *159* (2), 281–292.

(25) Sato, T.; Kadowaki, H.; Masuda, H.; Iio, K. Neutron Diffraction Study of Successive Phase Transitions in the Heisenberg Antiferromagnet $MnBr_2$. *J. Phys. Soc. Japan* **1994**, *63* (12), 4583–4596.

(26) McGuire, M. A. Crystal and Magnetic Structures in Layered, Transition Metal Dihalides and Trihalides. *Crystals* **2017**, *7* (5).

(27) Goodenough, J. B. *Magnetism and the Chemical Bond*; Interscience Publishers: New York, 1963.

(28) Kanamori, J. Superexchange Interaction and Symmetry Properties of Electron Orbitals. *J. Phys. Chem. Solids* **1959**, *10* (2–3), 87–98.

(29) Wiesler, D. G.; Suzuki, M.; Itsuko, S. S.; Rosov, N. Determination of Anomalous Superexchange in $MnCl_2$ and Its Graphite Intercalation Compound. *Phys. Rev. Lett.* **1995**, *75* (5), 942–945.

(30) Kahn, O. *Molecular Magnetism*; VCH Publishers: New York, 1993.

(31) Murugesu, M.; Takahashi, S.; Wilson, A.; Abboud, K. A.; Wernsdorfer, W.; Hill, S.; Christou, G. Large Mn_{25} Single-Molecule Magnet with Spin S = 51/2: Magnetic and High-Frequency Electron Paramagnetic Resonance Spectroscopic Characterization of a Giant Spin State. *Inorg. Chem.* **2008**, *47* (20), 9459–9470.

(32) Peverati, R.; Truhlar, D. G. M11-L: A Local Density Functional That Provides Improved Accuracy for Electronic Structure Calculations in Chemistry and Physics. *J. Phys. Chem. Lett.* **2012**, *3* (1), 117–124.

(33) Shoji, M.; Koizumi, K.; Kitagawa, Y.; Kawakami, T.; Yamanaka, S.; Okumura, M.; Yamaguchi, K. A General Algorithm for Calculation of Heisenberg Exchange Integrals J in Multispin Systems. *Chem. Phys. Lett.* **2006**, *432* (1–3), 343–347.

SYNOPSIS TOC (Word Style “SN_Synopsis_TOC”). If you are submitting your paper to a journal that requires a synopsis graphic and/or synopsis paragraph, see the Instructions for Authors on the journal’s homepage for a description of what needs to be provided and for the size requirements of the artwork.

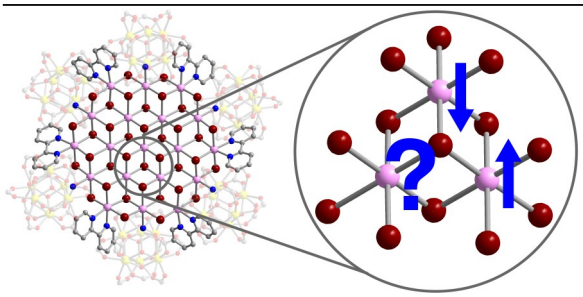

$Zr_6O_4(OH)_4(bpydc)_6(MnBr_2)_{19}$
